MOLECULAR IMAGING AND BIOLOGY

World Molecular Imaging Society

RESEARCH ARTICLE

Evaluation of [18F]-CP18 as a PET Imaging Tracer for Apoptosis

Helen Su, Gang Chen, Umesh Gangadharmath, Luis F. Gomez, Qianwa Liang, Fanrong Mu, Vani P. Mocharla, A Katrin Szardenings, Joseph C. Walsh, Chun-Fang Xia, Chul Yu, Hartmuth C. Kolb

Molecular Imaging Biomarker Research, Siemens Medical Solutions USA, Inc, 6100 Bristol Parkway, Culver City, CA, 90230, USA

Abstract

Purpose: We identified and validated [18F]-CP18, a DEVD (the caspase 3 substrate recognition motif) containing substrate-based compound as an imaging tracer for caspase-3 activity in apoptotic cells.

Procedures: CP18 was radiolabeled with fluorine-18 using click chemistry. The affinity and selectivity of CP18 for caspase-3 were evaluated *in vitro*. The biodistribution and metabolism pattern of [18F]-CP18 were assessed *in vivo*. [18F]-CP18 positron emission tomography (PET) scans were performed in a dexamethasone-induced thymic apoptosis mouse model. After imaging, the mice were sacrificed, and individual organs were collected, measured in a gamma counter, and tested for caspase-3 activity.

Results: In vitro enzymatic caspase-3 assay demonstrated specific cleavage of CP18. *In vivo*, [18F]-CP18 is predominantly cleared through the kidneys and urine, and is rapidly eliminated from the bloodstream. There was a sixfold increase in caspase activity and a fourfold increase of [18F]-CP18 retention in the dexamethasone-induced thymus of treated versus control mice.

Conclusions: We report the use [18F]-CP18 as a PET tracer for imaging apoptosis. Our data support further development of this tracer for clinical PET applications.

Key words: Apoptosis, Molecular imaging, PET, Caspase

Introduction

Apoptosis is a mode of programmed cell death critical for the development and maintenance of tissues and organs, and contributes to both normal physiology and pathology [1]. Disruption of the apoptosis pathway is believed to play a key role in a variety of human diseases, including cancer, cardiac ischemia, neurodegeneration, and others [2–6]. Therefore, the development of a noninvasive imaging procedure that can detect and monitor abnormal levels of apoptosis or follow apoptosis during treatments in a variety of disease states would be of tremendous value for providing diagnostic value and information for patient management. A positron emission tomography (PET) imaging agent targeting apoptosis is ideal for such a purpose as it is noninvasive, can track multiple lesions simultaneously, and can be used to follow treatment or disease progression.

Several strategies have been used for measuring and monitoring apoptosis. A commonly used apoptosis imaging target is phosphatidylserine (PS), a phospholipid that is externalized on the outer leaflet of the plasma membrane in the early stages of apoptosis [7]. Annexin V (also known as annexin A5) is a 36-kDa protein that selectively binds PS with high affinity. Annexin V has been labeled with different

isotopes for PET and single photon emission computed tomography (SPECT) imaging studies [8]. ^{99m}Tc-Annexin V imaging of apoptosis using SPECT showed promising results and is undergoing evaluation in clinical trials [9]. However, since the externalization of PS also occurs during necrosis, Annexin V alone cannot distinguish apoptotic from necrotic tissues either *in vitro* or *in vivo*. To resolve this, a secondary marker, such as propidium iodide, is required for in vitro deconvolution, but this strategy cannot be implemented *in vivo*.

An alternative approach is to target a more specific mediator of the apoptotic process, such as caspase activation [10]. Caspases are a family of intracellular cysteine proteases that are responsible for the regulation and execution of the apoptosis pathway. To date, 13 caspases have been identified and can be divided into two groups: initiator and effector caspases [11]. Caspases activated early in the process of apoptosis are known as initiator caspases, such as caspase-2, -8, -9, and -10. The function of these caspases is to activate the downstream effector caspases: caspase-3,–6, and -7, which are responsible for the proteolytic cleaveage of proteins that are necessary for cellular function. Although there are two different pathways for initiating apoptosis (i.e., the extrinsic and intrinsic pathways), both pathways converge at the level of capases-3 activation. Therefore, activated caspase-3 is an unambiguous marker for apoptosis.

Several fluorescent imaging probes have been developed for detecting caspase-3 activity [12, 13]; however, only a few caspase-based radiolabeled imaging agents have been successful. A number of non-peptidic, small molecule inhibitors utilizing the isatin sulfonamide scaffold target the active site of caspases-3 and -7 [14]. The utility of [^{18}F]-radiolabeled isatins as probes for PET imaging of apoptosis has been described [15–17], and further refinement for improving specific activity and reducing synthesis time has been reported [18]. These isatin-based radiotracers typically demonstrate poor metabolic stability. In addition, an important issue with these caspase inhibitors is that they usually lack target specificity, as they are also effective inhibitors of other cellular proteases (e.g., cathepsins and legumains) and are recognized and cleaved by active caspase-3.

We have developed an apoptosis imaging agent, [^{18}F]-CP18 (Fig. 1) as a substrate-based probe to detect caspase activity. Because caspase-3 has a substrate preference for the tetrapeptide motif Asp-Glu-X-Asp (DEXD) [19] and cleaves the peptide bond at the C-terminal of the aspartic acid residue, we designed [^{18}F]-CP18 to contain a "DEVD-A" penta-peptide motif. Several structural analogs were synthesized and tested. We found that incorporation of a short PEG chain resulted not only in higher uptake of the tracer in induced cells but also had better PK properties *in vivo*. There are some reports that PEG chains might enhance cell permeability [20, 21], but it is difficult to delineate the contributions of each structural element of a molecule as complex as CP18. Mechanistically, [^{18}F]-CP18 freely permeates cell membranes, and in cells that have little to no intracellular caspase-3 activity, there is no preferential retention of [^{18}F]-CP18. However, after [^{18}F]-CP18 is recognized and cleaved by intracellular caspase-3, it loses the C-terminus PEG chain, which renders it unable to permeate the cell membrane, and results in the preferential cellular retention of the radiolabeled metabolite (Fig. 2). [^{18}F]-CP18 is readily radiolabeled through the Cu(I)-catalyzed Huisgen reaction ("click chemistry"). This is an ideal reaction for [^{18}F] radiolabeling of a complex peptide analog such as CP18 since it is fast, high-yielding, highly selective, and requires minimal use of protecting groups [22–24]. In this study, we describe the radiolabeling of [^{18}F]-CP18 and investigated the ability of [^{18}F]-CP18 to image apoptosis noninvasively. We evaluated the affinity and selectivity of [^{18}F]-CP18 for caspase-3 using *in vitro* enzymatic and cellular assays. Its biodistribution and metabolism pattern were also assessed *in vivo*. Finally, the uptake of [^{18}F]-CP18 in rodents with chemically induced apoptotic thymii was validated.

Materials and Methods

Chemical Synthesis and Radiolabeling

The CP18 precursor was synthesized using standard peptide chemistry and intermediates as described in the literature in eight steps. Detailed procedures and analytical data for each intermediate and the precursor are provided in detail in the Electronic Supplemental Material (ESM). The standard was prepared via copper-catalyzed click chemistry in 84 % from the azide-containing precursor and fluoropentyne.

The [^{18}F]-CP18 tracer was prepared on an automated synthesis module ("Explora RN" from Siemens). A solution of the tosylate precursor in THF was added to the reaction vessel containing the anhydrous [^{18}F]fluoride to generate [^{18}F]fluoropentyne. The [^{18}F]fluoropentyne was distilled from the reaction vessel into the click mixture containing the azide CP18 precursor, CuSO4, TBTA, and sodium ascorbate in DMF and MeOH. After HPLC purification, [^{18}F]-CP18 was captured on a C18 SepPak cartridge and the tracer eluted with ethanol. The final formulation contained a maximum of 10 % ethanol:90 % water (*v/v*). [^{18}F]-CP18 was obtained in an average radioactive yield of 40 % with an average synthesis time of 92 min and average specific activity of 1.75×10^5 MBq/µmol.

Enzymatic Caspase-3 Assay

CP18 (2 nmol) was incubated with 0.25 U of human recombinant caspase-3 (Millipore, MA) in 200 µl of assay buffer (50 mM HEPES, pH 7.4, 100 mM NaCl, 0.1 % CHAPS, 1 mM EDTA, 10 mM DTT, 10 % glycerol). Twenty microliters of sample were collected at 30, 60, 90, and 120 min and analyzed by liquid chromatography mass spectrometry (Agilent Technologies, Santa Clara, CA) at 37° using the HPLC column Eclipse XDB-C18 (Agilent Technologies, Santa Clara, CA). The area under the curve for unchanged CP18 (exact mass, 1,153.12) and the cleaved product (exact mass, 645.59) was determined. The cleavage rate of substrate was expressed as the percentage of the cleaved CP18 product over total CP18 per hour per unit caspase-3 enzyme.
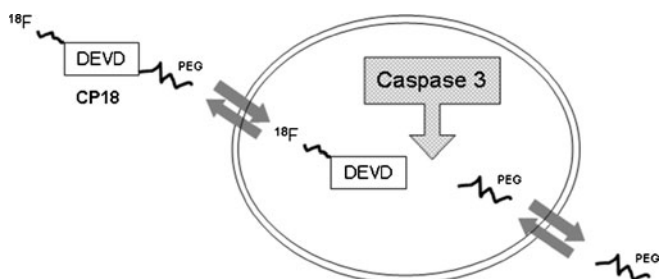
Fig. 1. Schematic representation of the mechanism for [^{18}F]-CP18 cell uptake.

Cell Uptake Assay of CP18

U87 and A427 cells, obtained from ATCC (Manassas, VA), were cultured in EMEM (ATCC) supplemented with 10 % fetal bovine serum, 100 units/ml of penicillin, and 100 units/ml of streptomycin (Invitrogen, Carlsbad, CA). Cells were grown at 37°C in an atmosphere of 5 % CO_2. U87 and A427 cells were plated in six-well plates and treated with 1 mM of 5-fluorouracil (5-FU) for 2 days, while the control group was left untreated. All cells were then exposed to 10 μM of CP18 for 2 h and harvested by filter filtration. The filters were rinsed and placed in cell lysis buffer (0.2 % SDS in PBS). The lysates were then deproteinated with chloroform/methanol (1:1) and centrifuged at full speed. The supernatant in the upper phase was collected and analyzed by liquid chromatography mass spectrometry (Agilent Technologies, Santa Clara, CA) using the HPLC column Eclipse XDB-C18 (Agilent Technologies, Santa Clara, CA) for detection of the parental form as well as the metabolites of CP18.

Animals

CD1 mice were purchased from Harlan (Indianapolis, IN). All animal experiments were conducted in compliance with the guidelines approved by the Institutional Animal Care and Use Committee of Siemens Healthcare.

Biodistribution

Male CD1 mice were anesthetized with 2–3 % isoflurane/97–98 % oxygen, and ~7.4 MBq [^{18}F]-CP18 in ~8 % ethanol, and deionized water was administered via bolus intravenous tail vein injection. Conscious uptake of the radioactive tracer was performed until at the indicated time points, mice were anesthetized again, and whole blood was collected into EDTA-containing tubes via cardiac puncture. The anticoagulated blood was then centrifuged to separate plasma from red blood cells. In addition, urine was collected via cystocentesis. The mice were then euthanized and the liver, kidneys, muscle, brain, and heart were harvested and weighed. Tissue samples were counted in a Wallac Wizard Gamma counter (Perkin-Elmer, Waltham, MA). All data were decay corrected and represented as percentage of injected dose per gram.

Biostability

~9.25 MBq of [^{18}F]-CP18 was injected via the tail-vein into CD1 mice. The animals were sacrificed at 30 min ($n=3$) and 60 min ($n=3$) post-injection. Whole blood was obtained, weighed, and centrifuged to isolate plasma, which was then mixed with an equal volume of lysis buffer (0.2 % SDS in PBS). Urine was also collected and mixed with an equal volume of lysis buffer. The brain, kidneys, and liver were harvested, weighed, and homogenized in lysis buffer. Four hundred microliters of each sample was subsequently removed, mixed with an equal volume of chloroform/methanol (1:1), vigorously vortexed, and placed on dry ice for 3 min. After thawing, another centrifugation step at 13,000RPM (7 min) allowed for the separation of organic ($CHCl_3$) and aqueous ($MeOH/H_2O$) fractions. The organic and aqueous fractions were then removed and counted in a Wizard gamma counter (Perkin-Elmer, Waltham, MA). The samples were also analyzed by HPLC, using a radiometric detector (Agilent Technologies, Santa Clara, CA). All data were decay corrected and represented as percentage of injected dose per gram.
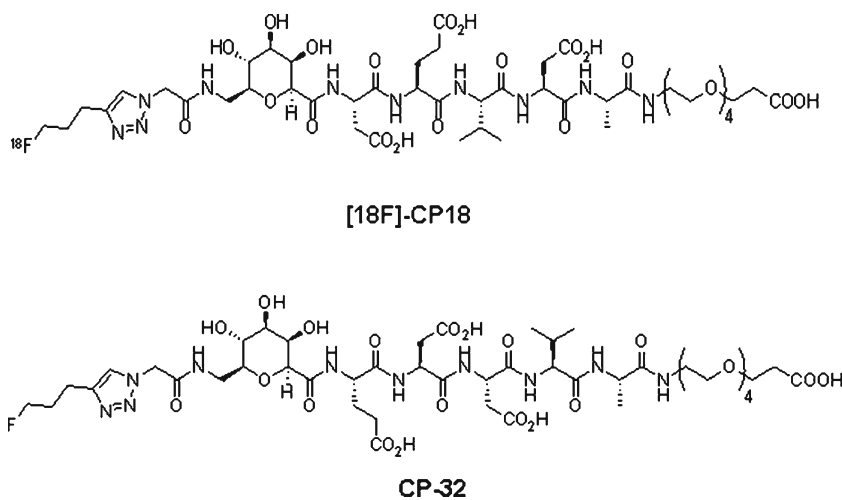

[18F]-CP18

CP-32

Fig. 2. Structure of [^{18}F]-CP18 and CP32.

In Vivo Thymus Apoptosis Model

Dexamethasone sodium phosphate (Sigma, St. Louis, MO) was formulated in saline, and administered to 4–6-week-old female CD-1 mice (Harlan, Indianapolis, IN) at 250-μl intraperitoneal (i.p.) injections of 4 mg/ml doses (~1 mg/mouse). Age-matched mice were used for the control group, which received i.p. injections of saline. Nine hours later, a dose of ~7.4 MBq/mouse (in 100–200 μl saline) of [^{18}F]-CP18 or [^{18}F]-CP32 was administered through tail vein injection ($n=5$). Mice were then subjected to microPET/CT scanning, before being sacrificed at 90 min after tracer injection. Tissues from the thymus and muscle were collected and weighed. The radioactivity in the tissue samples was then measured in a Beckman Gamma Counter (Brea, CA). Sample radioactivity was counted at the same time, thus eliminating the need for radioactivity decay correction. The amount of tracer in each tissue is expressed as percentage of injected dose per gram. Samples were immediately stored at −80 °C after they were measured in the gamma counter. The next day, samples were thawed, lysed, and homogenized in T-PER buffer (Fisher, Pittsburgh, PA) on ice followed by measuring caspase-3 activity. Similar procedures were performed on the control group ($n=5$), which received saline injections (250 μl i.p. injection) instead of dexamethasone.

MicroPET/CT Imaging

An INVEON Multimodality scanner (Siemens) was used for microPET/CT imaging. Mice were anesthetized with 2–3 % isoflurane/97–98 % oxygen, and placed on a heated scanner bed during the imaging session. A 7-min CT scan was first performed for anatomical registration followed by a 15-min static PET scan or a 120-min dynamic scan. Images were reconstructed using filtered backprojections without attenuation, scatter, or dead-time corrections. Quantification of tracer uptake was performed by visually drawing regions of interest (ROI) based on the fused PET/CT images, and the corresponding activity values were determined using the INVEON Research Workplace software (Siemens). All values are represented as percent injected dose per gram.

Caspase-3 Activity Assay in Lysates

Cell pellets or tissue homogenates were first lysed in T-PER buffer (Fisher, Pittsburgh, PA). A fluorogenic caspase-3 substrate, Ac-DEVD-AFC (AnaSpec, CA), was added to the lysate in a 1-mM DTT-containing 2× reaction buffer (150 mM MaCl, 50 mM HEPES, 5 mM EDTA, 1 mM DTT, 10 % glycerol, pH 7.0). The fluorogenic reaction was read in a SpectraMax M2 plate reader (Molecular Devices, CA) at 405 nm wavelength every 5 min for 2 h. Caspase-3 activity was calculated as the amount of AFC detected per minute per milligram of protein. Protein concentrations were measured by Bradford assay (Bio-Rad, CA).

Thymus Metabolism

For the metabolite analysis, thymi from dexamethasone-treated and control groups were removed 30 min after [^{18}F]-CP18 administration and lysates prepared from three animals/group with TPER buffer (1:1

wt of organ/buffer). Plasma was also collected from both treated and control groups. The samples (thymi and plasma) were processed by adding 25 μl of 8 % acetic acid in acetonitrile/100 μl of the lysate or plasma, vortexed at high speed for 1 min, cooled on ice for 3 min, thawed, and centrifuged at 30,000 rpm. After separating from the pellet, the supernatant sample was injected on an HPLC using a radiometric detector (Agilent Technologies, Santa Clara, CA).

Statistical Analysis

Results are expressed as mean+SD. Student's T test was used for comparisons between unpaired data. ANOVA was used to compare tracer uptake and caspase activity in the thymus versus muscle and liver. All analyses were performed using the Graphpad Prism software (La Jolla, CA).
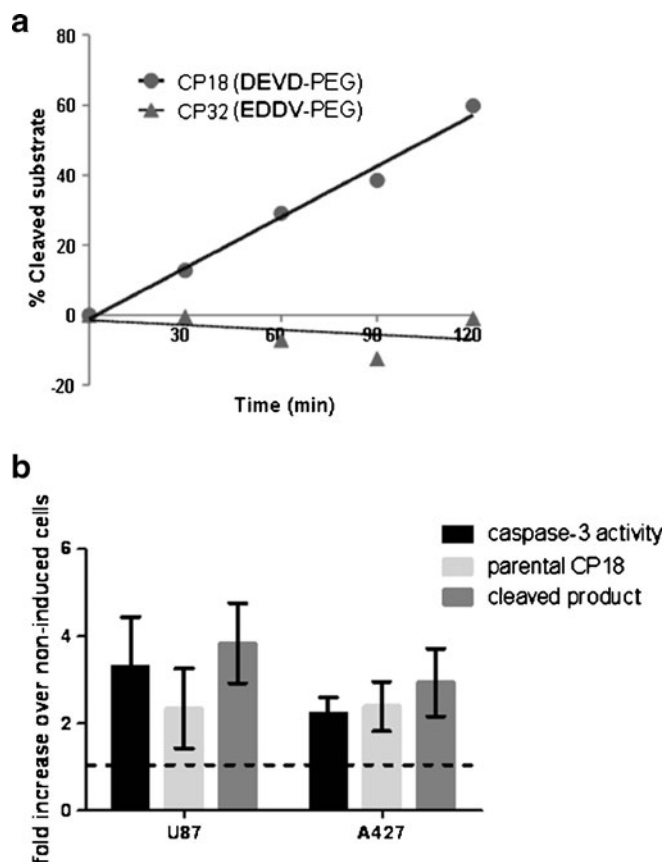
Results

Synthesis and Radiolabeling of CP18

CP18 and its analogous peptides were prepared via multi-step syntheses (see ESM). The CP18 precursor was prepared in eight steps with a combined yield of 15 %, whereas the cold CP18 standard was readily prepared using copper sulfate/sodium ascorbate-catalyzed click chemistry conditions from the precursor with 84 % yield. The radiosynthesis of [^{18}F]-CP18 was readily accomplished using the Cu(I)-catalyzed click reaction, even in the presence of the different functional groups present in the molecule. The labeling was accomplished with an average synthesis time of 92 min, which is less than one half-life of [^{18}F] fluorine. The average radioactive yield was 40 % (decay corrected), and the average specific activity was 1.75×10^5 MBq/μmol, making this production protocol adequate for preclinical studies. The tracer was stable in solution at high strength (>925 MBq/ml) for up to 8 h after the end of synthesis.

In Vitro Evaluation of CP18

An *in vitro* caspase-3 assay was used to confirm that CP18 is a substrate for caspase-3. When CP18 was incubated in the presence of recombinant caspase-3, there was both a loss of parent CP18 and a corresponding increase of the cleavage product. The cleavage product, which we confirmed to be "DEVD," increased over time, at a rate of 1.60 nmol/h per U of caspase-3 (Fig. 3a). To verify the specificity of cleavage by caspase-3, no cleavage products were detected when using a negative control analog, CP32, which contains a scrambled recognition sequence ("EDDV") instead of the DEVD motif. As expected, CP32 was not cleaved by caspase-3 (Fig. 3a), thus confirming the selective cleavage of CP18 in the presence of activated caspase-3. The negative values are due to a slight increase of the parent CP32 signal, which could be due to more CP32 being dissolved over time under the experimental conditions.
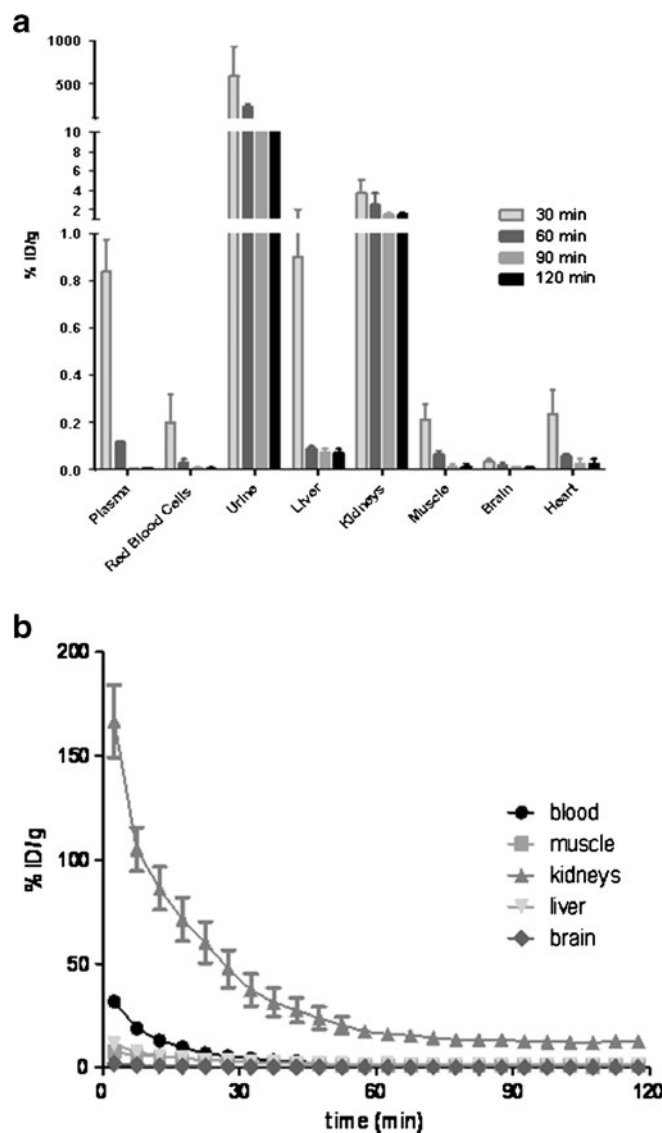
Fig. 3. **a** *In vitro* enzymatic caspase-3 assay ($n=3$). Amount of cleaved products is shown as percentage of total parental substrate, and analyzed for linear regression, resulting in $r^2 = 0.98$ for CP18 and $r^2 = 0.16$ for CP32. **b** Cell uptake assay. The results are shown as fold increase over control±SD. The *dashed line* drawn at onefold increase over control represents no difference between induced versus control group. *Numbers above the line* indicate an increase compared to control, whereas *numbers below the line* represent a decrease over control.

Fig. 4. Biodistribution and time activity curve of [¹⁸F]-CP18 in CD1 mice. **a** Selected tissues were collected at each time point ($n=3$). Data are expressed as percentage of injected dose per gram tissue±SD. **b** Dynamic PET/CT scans were performed on CD1 mice ($n=3$), and ROIs were drawn around the indicated tissues. The PET signal is represented as percentage of injected dose per gram.

CP18 was found to accumulate selectively in cultured cells undergoing apoptosis. Both U87 and A427 cells were treated in culture with 5-FU to induce apoptosis and activate caspase-3 (two- to threefold increase, Fig. 3b). After incubating the cells for 2 h in the presence of CP18, there was ~2-fold increase of intracellular parental CP18 and ~3-fold increase of cleaved product in both cell lines, demonstrating that cellular retention of CP18 was induced by caspase-3-dependent apoptosis. No difference in preferential uptake was observed when CP32 was incubated with cells induced with 5-FU (data not shown).

In Vivo Evaluation of CP18

The biodistribution pattern of [¹⁸F]-CP18 in CD1 mice ($n=3$) indicated that the predominant clearance pathway for this tracer is via the kidneys (Fig. 4a). There was also a significant amount of [¹⁸F]-CP18 in the gallbladder, suggesting some hepatobiliary clearance of the tracer, but the uptake of the tracer in the liver was relatively low. The fast clearance rate of the tracer from the blood into the urine was beneficial for ensuring low background uptake of the tracer. Similar biodistribution patterns were observed in [¹⁸F]-CP18 dynamic scans on CD1 mice ($n=3$), in which the time activity curve demonstrated a fast clearance of the tracer by 60 min (Fig. 4b).

[¹⁸F]-CP18 exhibited a favorable *in vivo* biostability profile in mice up to 60 min post-injection. The percentage of injected dose per gram values for CHCl₃ (organic) and MeOH/water (aqueous) fractions and for the total organ are

Table 1. *In vivo* biostability of [18F]CP-18

Time post-Injection (min)	%ID/g								
	Kidney			Plasma			Urine		
	MeOH	CHCl3	Total	MeOH	CHCl3	Total	MeOH	CHCl3	Total
[18F]-CP18									
30	0.76	0	0.76	1.65	0.52	2.17	20.14	21.57	41.71
60	0	0	0	0.14	0	0.14	31.41	27.81	59.22
[18F]-DE									
30	1.3	0	1.3	0	0.06	0.06	2.67	2.82	5.49
60	0	0	0	0	0	0	4.07	3.97	8.04
[18F]-DEVD									
30	0	0	0	0	0	0	1.46	1.28	2.74
60	0	0	0	0	0	0	1.48	1.32	2.8

listed in Table 1. There are two predominant metabolites, detected with shorter retention times of 11.07 and 11.8 min, whereas the retention time for [18F]-CP18 is 12.98 min. Based on their retention time, we identified the two metabolites as the [18F]-DE fragment and the [18F]-DEVD fragment. Both metabolites were cleared primarily through the kidneys and into the urine. The plasma samples at 30 min post-injection contained predominantly intact [18F]-CP18 (93 %; 2.17 % ID/g) and a minor amount of [18F]-DE (7 %; 0.06 %ID/g). There was no detectable activity present in the plasma samples at 60 min. In the kidneys, the tracer was 37 % intact (0.76 %ID/g) along with 63 % of [18F]-DE (1.3 %ID/g) at 30 min post-injection. The urine samples contained 40 and 60 % ID/g of the intact [18F]-CP18 at 30 and 60 min, respectively. Both metabolites were present in the urine samples with [18F]-DE increasing from 5.49 to 8.04 % ID/g at 30 and 60 min. The amount of [18F]-DEVD remained constant over time at 2 % ID/g. No activity was detected in either the brain or liver samples.

Applying [18F]-CP18 to an In Vivo Apoptosis Model

The uptake of [18F]-CP18 was determined in the well-characterized thymus mouse model of apoptosis, induced by the administration of dexamethasone. This model was ideal because the kinetics of apoptosis have been explored in previous studies using a number of common apoptosis markers including TUNEL and Annexin V [25, 26]. The optimal timing of dexamethasone-induced apoptosis in the thymi was at 10.5 h post-dexamethasone treatment and was confirmed by the detection of a six- to tenfold increase in caspase-3 activity in the apoptotic thymi (data not shown). Therefore, mice ($n=5$) were injected with [18F]-CP18 at 9 h post-dexamethasone treatment and microPET-CT scanned at 90 min post-tracer injection (Fig. 5a). Given the small size of the mouse thymus and the limited resolution of the PET scanner, we were gratified to obtain a PET image at all. A maximum intensity projection image of the PET-CT scan of the treated mouse is shown in Fig. 3S in the ESM. A [18F]-CP18 signal was detected in the thymus of treated mice but not in the control group. PET signal quantitation of the thymi revealed a 5.1-fold difference of signal between treated and control mice (Fig. 5b). We also PET/CT scanned a separate group of dexamethasone-treated mice with the negative control tracer, [18F]-CP32, and detected ~2-fold less signal compared to treated mice scanned with [18F]-CP18. To further confirm PET results, the animals ($n=5$) were then sacrificed, and caspase levels were measured along with tracer uptake (Fig. 5c) in the thymus and muscle (results represented as percentage of injected dose per gram are listed in Table 1S in the ESM). A corresponding 4.3-fold increase of [18F]-CP18 uptake and 1.9-fold increase of [18F]-CP32 uptake in the apoptotic thymus were observed as compared to control. Little to no change in caspase activity and tracer retention in the muscle in treated versus control mice was found.

The cleavage products/metabolites of [18F]-CP18 in the thymus of the dexamethasone-treated mice were further analyzed (Fig. 6). The HPLC analysis of thymi lysates obtained 30 min post-injection of tracer showed complete conversion of parent [18F]-CP18 into the two metabolites as seen previously, but only a low level of intact CP18 was found in the thymi of non-treated control group. Plasma samples from both the induced and control group animals showed mostly intact [18F]-CP18 and very small amounts of [18F]-DE. Therefore, the CP18 fragments detected in the induced animals must have come from CP18 cleaved in the thymus.

Discussion

In this study, we demonstrate the potential of using [18F]-CP18 as a PET tracer for imaging caspase-3 activity in cells undergoing apoptosis. *In vitro* cleavage assays using activated caspase-3 confirmed that CP18, which contains the caspase-3 substrate binding motif ("DEVD"), is a specific substrate for caspase-3. Against other proteases, CP18 demonstrated poor binding affinity further confirming its selectivity for caspase-3. Moreover, CP18 and its
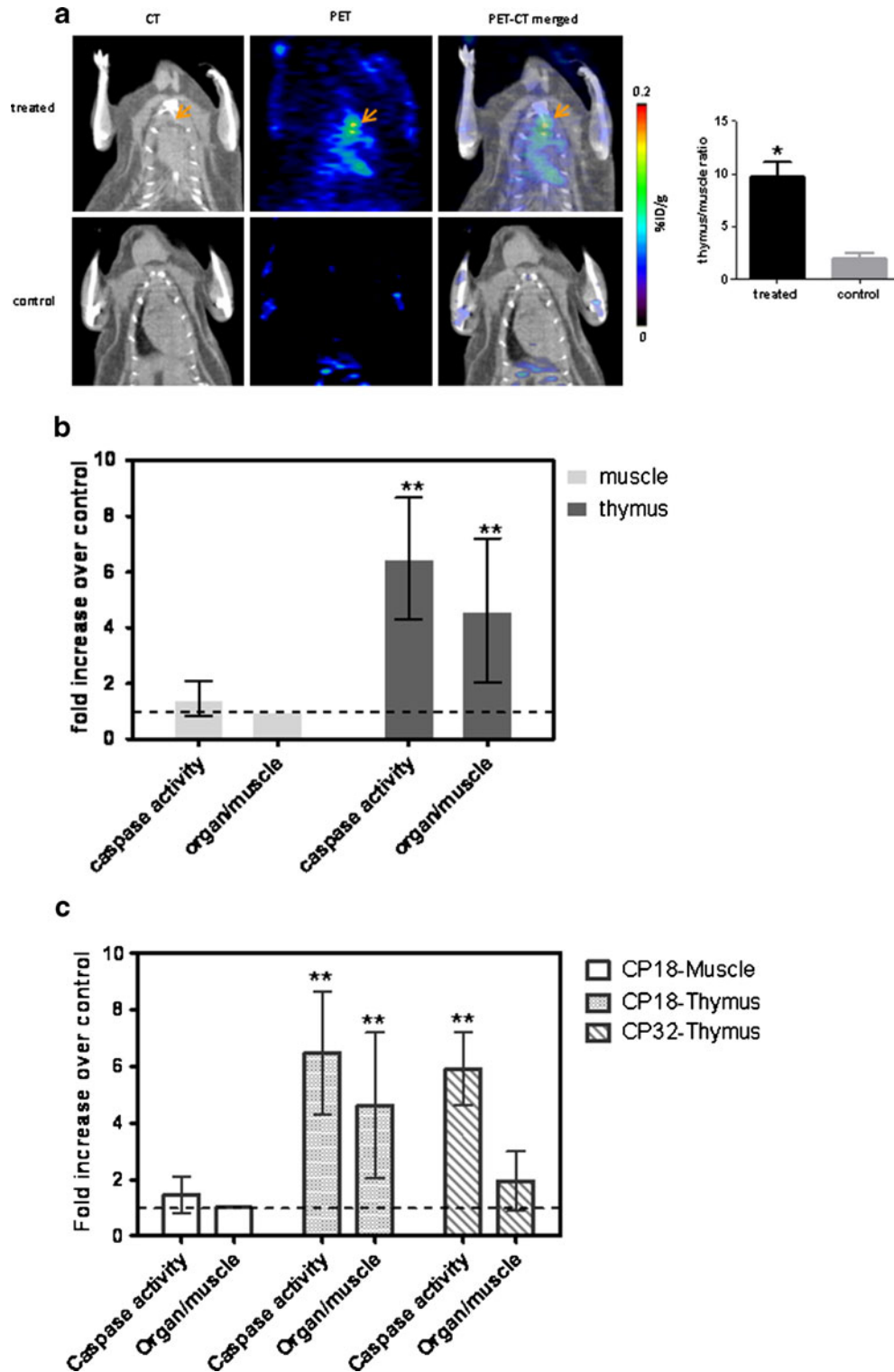
Fig. 5. CP18 in dexamethasone-induced thymus apoptosis. **a** Treated and control mice ($n=5$) were administered with [¹⁸F]-CP18 or [¹⁸F]-CP32 and PET/CT scanned. ROIs were drawn around the thymus and quadriceps muscle, and **b** PET signal was quantified and normalized as thymus-over-muscle ratio. *$P<0.05$. **c** Animals were then sacrificed and various organs collected to determine the level of CP18 and caspase ($n=5$). CP18 levels were determined by measuring the amount of radioactivity in the organs *ex vivo* and normalized to the radioactivity amount in the reference tissue (i.e., muscle). The data were then compared to the results from the control group, and represented as fold increase over control±SD. The *dashed line* drawn at onefold increase over control represents no difference between induced versus control group. *Numbers above the line* indicate an increase compared to control, whereas *numbers below the line* represent a decrease over control. **$P<0.0001$.
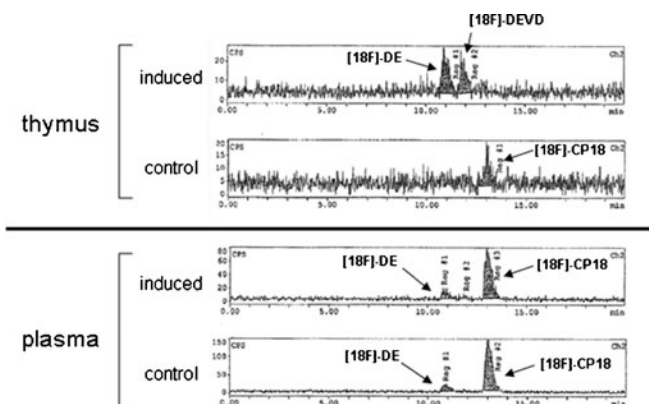
Fig. 6. Metabolite analysis in thymi from mice injected with [^{18}F]-CP18. HPLC traces are shown for dexamethasone-induced thymus apoptosis and control animals at 30 min posttreatment. A relative percentage of each fragment is given for each HPLC trace.

metabolites were selectively retained in apoptotic cells induced by treatment with 5-FU. Non-induced cells contained only a baseline level of intact CP18. *In vivo*, [^{18}F]-CP18 exhibited a favorable biodistribution and clearance profile, as well as favorable metabolic stability, especially in plasma affording a low background signal *in vivo*. In a mouse model of dexamethasone-induced thymic apoptosis, an enhanced retention of the [^{18}F]-CP18 metabolites was detected in the thymi of treated versus control mice, consistent with the proposed mechanism of intracellular localization. Additionally, the uptake of the tracer correlated linearly with caspase expression levels ($r^2 = 0.9102$), additionally validating the ability of using [^{18}F]-CP18 as a PET tracer to detect and image apoptotic tissues.

Several radioligands have been developed for imaging apoptosis. Annexin V [27], C2A [28], duramycin [29], and the ApoSense markers [30, 31] are all designed to target the plasma membrane of apoptotic cells. Another approach for developing apoptosis imaging agents is to target caspase enzymes by using either caspase inhibitors or caspase substrates. Several isatin sulfonamide analogs have been identified to have nanomolar potency for inhibiting the caspase-3 and -7 enzymes, and have been radiolabeled for use as PET imaging tracers [15–17]. A common problem for isatin-based tracer is that caspase inhibitors usually lack specificity, as they are also effective inhibitors of various cathepsins. An irreversible caspase inhibitor and its optimal sequence for specificity have been identified [32]. Optical imaging probes were developed by conjugating this sequence with near-infrared fluorescent tags and a cell-permeable peptide sequence [32].

The second method for direct caspase imaging is to utilize caspase substrates. Since effector caspases are known to recognize the DEXD motif, several optical imaging probes have been designed to include this sequence [33–38]. The integration of the DEXD motif enhances specificity

of probes such that they are cleaved only by active caspases, which results in relative low background activity. Several others have reported the use of DEVD for optical imaging of caspase activity [33–36]; however, there have been limited reports regarding the radiolabeling of this type of tracer for PET imaging [37, 38]. We designed CP18 to contain the DEVD substrate sequence, along with a N-terminus galactose fragment and C-terminus PEGylation for enhancement of cell penetration of the tracer. Click chemistry was an obvious choice for radiolabeling this type of multi-functional peptidic compound [39].

A common observation in the specificity of using DEVD-based probes to monitor caspase activity is the cathepsin-mediated recognition and digestion of DEVD, which results in intracellular signal retention even in non-apoptotic cells. This cross-reaction results in nonspecific cleavage and may potentially increase the background activity during *in vivo* imaging. In our cell uptake assay, the parental CP18 uptake in apoptotic cells was higher compared to non-induced cells, indicating the presence of non-specific uptake of the tracer. Nevertheless, since cell culture results do not always translate well to *in vivo* situations, we directly addressed the issue by comparing in vivo PET/CT scans using [^{18}F]-CP18 with [^{18}F]-CP32 (Fig. 5). We detected a slight nonspecific uptake of [^{18}F]-CP32 in the apoptotic thymi. However, this background signal is approximately twofold less than [^{18}F]-CP18 signals (detected by both PET and gamma counting).

The mechanism of the nonspecific uptake of CP18 is currently unknown. From our biostability assays both in cells and *in vivo*, we found two metabolites or cleaved products from CP18: the expected cleaved product of DEVD, and also a smaller fragment, DE. We speculate that this smaller fragment is likely the result of further proteolysis of the cleaved product DEVD by a yet to be identified protease. Further experiments are needed to verify this. Nonetheless, we do not believe that the presence of the smaller cleaved product, "DE," affects the specificity of CP18 and its utility for imaging apoptosis. However, further investigations into the exact mechanism for the nonspecific uptake are needed to improve this class of tracer.

Conclusion

We report here the utility of [^{18}F]-CP18 as a PET tracer for imaging apoptosis by detecting activated caspase-3. The specificity of CP18 *in vitro* and in cell cultures was validated, and favorable biodistribution properties and metabolic stability of CP18 were demonstrated *in vivo*. Finally, a high correlative retention of [^{18}F]-CP18 in dexamethasone-induced apoptotic thymi was observed, thus confirming the ability of using CP18 to detect apoptosis *in vivo*. Since apoptosis plays a major role in many diseases, the ability to quantify and monitor this process may play a critical role in both diagnosis and patient management. This can benefit a multitude of

clinical disorders including stroke, pulmonary inflammatory diseases, myocardial ischemia and inflammation, organ transplantation, and oncology.

References

1. Jacobson MD, Weil M, Raff MC (1997) Programmed cell death in animal development. Cell 88:347–354
2. Thompson C (1995) Apoptosis in the pathogenesis and treatment of disease. Science 267:1456–1462
3. Rimon G, Bazenet CE, Philpott KL, Rubin LL (1997) Increased surface phosphatidylserine is an early marker of neuronal apoptosis. J Neurosci Res 48:563–570
4. Olivetti G, Abbi R, Quaini F et al (1997) Apoptosis in the failing human heart. N Engl J Med 336:1131–1141
5. Krams SM, Martinez OM (1998) Apoptosis as a mechanism of tissue injury in liver allograft rejection. Semin Liver Dis 18:153–167
6. Darzynkiewicz Z (1995) Apoptosis in antitumor strategies: modulation of cell cycle or differentiation. J Cell Biochem 58:151–159
7. Blankenberg FG, Katsikis PD, Tait JF et al (1998) In vivo detection and imaging of phosphatidylserine expression during programmed cell death. Proc Natl Acad Sci U S A 95:6349–6354
8. Lahorte CMM, Vanderheyden J, Steinmetz N et al (2004) Apoptosis-detecting radioligands: current state of the art and future perspectives. Eur J Nucl Med Mo Imaging 31:887–919
9. Kemerink GJ, Liu X, Kieffer D et al (2003) Safety, biodistribution, and dosimetry of 99mTc-HYNIC-annexin V, a novel human recombinant annexin V for human application. J Nucl Med 44:947–952
10. Grütter MG (2000) Caspases: key players in programmed cell death. Curr Opin Struct Biol 10:649–655
11. Shi Y (2004) Caspase activation, inhibition, and reactivation: a mechanistic view. Protein Sci 13:1979–1987
12. Blankengerg FG, Norfray JF (2011) Multimodality molecular imaging of apoptosis in oncology. AJR Am J Roentgenol 197:308–317
13. Kim K, Lee M, Park H et al (2006) Cell-permeable and biocompatible polymeric nanoparticles for apoptosis imaging. J Am Chem Soc 128:3490–3491
14. Chu W, Zhang J, Zeng C et al (2005) N-benzylisatin sulfonamide analogues as potent caspase-3 inhibitors: synthesis, *in vitro* activity, and molecular modeling studies. J Med Chem 48:7637–7647
15. Zhou D, Chu W, Chen DL et al (2009) [18F]- and [11C]-labeled N-benzyl-isatin sulfonamide analogues as PET tracers for apoptosis: synthesis, radiolabeling mechanism, and *in vivo* imaging study of apoptosis in Fas-treated mice using [11C]WC-98. Org Biomol Chem 7:1337–1348
16. Zhou D, Chu W, Rothfuss J et al (2006) Synthesis, radiolabeling, and in vivo evaluation of an 18F-labeled isatin analog for imaging caspase-3 activation in apoptosis. Bioorganic & Medicinal Chemistry Letters 16:5041–5046
17. Nguyen Q, Smith G, Glaser M et al (2009) Positron emission tomography imaging of drug-induced tumor apoptosis with a caspase-3/7 specific [18F]-labeled isatin sulfonamide. Proc Natl Acad Sci U S A 106:16375–16380
18. Nguyen Q, Challapalli A, Smith G et al (2012) Imaging apoptosis with positron emission tomography: "Bench to bedside" development if the caspase 3/7 specific [18F] ICMT-11. Eur J Cancer 48:432–440
19. Thornberry NA, Rano TA, Peterson EP et al (1997) A combinatorial approach defines specificities of members of the caspase family and granzyme B functional relationships established for key mediators of apoptosis. J Biol Chem 272:17907–17911
20. Dutot L, Lécorché P, Burlina F et al (2010) Glycosylated cell-penetrating peptides and their conjugates to a proapoptotic peptide: preparation by click chemistry and cell viability studies. J Chem Biol 3:51–65
21. Nguyen J, Xie X, Neu M et al (2008) Effects of cell-penetrating peptides and pegylation on transfection efficiency of polyethylenimine in mouse lungs. J Gene Med 10:1236–1246
22. Kolb HC, Finn MG, Sharpless KB (2001) Click chemistry: diverse chemical function from a few good reactions. Angew Chem Int Ed 40:2004–2021
23. Rostovtsev VV, Green LG, Fokin VV et al (2002) A stepwise Huisgen cycloaddition process: copper(I)-catalyzed regioselective "ligation" of azides and terminal alkynes. Angew Chem Int Ed 41:2596–2599
24. Tornoe CW, Christensen C, Meldal M (2002) Peptidotriazoles on solid phase: [1–3]-triazoles by regiospecific copper(I)-catalyzed 1,3-dipolar cycloadditions of terminal alkynes to azides. J Org Chem 67:3057–3064
25. Cifone MG, Migliorati G, Parroni R et al (1999) Dexamethasone-induced thymocyte apoptosis: apoptotic signal involves the sequential activation of phosphoinositide-specific phospholipase C, acidic sphin-gomyelinase, and caspases. Blood 93:2282–2296
26. Chmielewski V, Drupt F, Morfin R (2000) Dexamethasone-induced apoptosis of mouse thymocytes: prevention by native 7alpha-hydrox-ysteroids. Immunol Cell Biol 78:238–246
27. Faust A, Hermann S, Wagner S et al (2009) Molecular imaging of apoptosis in vivo with scintigraphic and optical biomarkers—a status report. Anti-Cancer Agents in Med Chemistry 9:968–985
28. Zhao M, Zhu X, Ji S et al (2006) 99mTc-labeled C2A domain of synaptotagmin I as a target-specific molecular probe for noninvasive imaging of acute myocardial infarction. J Nuc Med 47:1367–1374
29. Zhao M, Li Z, Bugenhagen (2008) 99m Tc-Labeled duramycin as a novel phosphatidylethanolamine-binding molecular probe. J Nuc Med 49:1345–1352
30. Damianovich M, Ziv I, Heyman SN et al (2006) ApoSense: a novel technology for functional molecular imaging of cell death in models of acute renal tubular necrosis. Eur J Nucl Med Mol Imaging 33:281–291
31. Hoglund J, Shirvan A, Antoni G et al (2011) 18F -ML-10, a PET tracer for apoptosis: first human study. J Nucl Med 52:720–725
32. Edginton LE, Berger AB, Blum G et al (2009) Noninvasive optical imaging of apoptosis by caspase-targeted activity-based probes. Nat Med 15:967–973
33. Niers JM, Kerami M, Pike L et al (2011) Multimodal *in vivo* imaging and blood monitoring of intrinsic and extrinsic apoptosis. Mol Ther 19:1090–1096
34. Scabini M, Stellari F, Cappella P et al (2011) *In vivo* imaging of early stage apoptosis by measuring real-time caspase-3/7 activation. Apoptosis 16:198–207
35. Hickson J, Ackler S, Klaubert D et al (2010) Noninvasive molecular imaging of apoptosis in vivo using a modified firefly luciferase substrate. Z-DEVD-aminoluciferin Cell Death Differ 17:1003–1010
36. Maxwell D, Chang Q, Zhang X et al (2009) An improved cell-penetrating, caspase-activatable, near-infrared fluorescent peptide for apoptosis imaging. Bioconjug Chem 20:702–709
37. Xiong C, Yang Z, Zhang R et al (2009) 99mTc-labeled Ac-DEVD peptides as a substrate for measuring caspase activity. Adv Exp Med Biol 611:455–456
38. Bauer C, Bauder-Wuest U, Mier W et al (2005) 131I-labeled peptides as caspase substrates for apoptosis imaging. J Nucl Med 46:1066–1074
39. Walsh J, Kolb H (2010) Applications of click chemistry in radiopharmaceutical development. Chimia 64:29–33